INTERNATIONAL JOURNAL FOR NUMERICAL METHODS IN FLUIDS, VOL. 17, 1079–1096 (1993)

ENTRANCE FLOW IN ELLIPTICAL DUCTS

K. VELUSAMY

Thermal Hydraulics Section, Indira Gandhi Centre for Atomic Research, Kalpakkam 603102, India

AND

VIJAY K. GARG

Internal Fluid Mechanics Division, NASA Lewis Research Center, Mail Stop 5-11, Cleveland, OH 44135, U.S.A.

SUMMARY

A control volume-based solution of the complete set of Navier–Stokes equations for the laminar, three-dimensional developing flow in elliptical cross-section ducts is described. Numerical results for velocity and pressure development, pressure defect and entrance lengths are presented for a wide range of aspect ratios from 0·1 to 0·999. The present results match very well with earlier numerical solutions for developing flow in a circular duct and the fully developed flow in elliptical ducts. A comparison with earlier numerical and experimental data for developing flow in elliptical ducts is also satisfactory for pressure development but not so good for the velocity profiles. The relative growth rate of boundary layer thickness along the major axis is slower than that along the minor axis which is contrary to the assumption used in earlier numerical analyses. The present results show no transverse recirculation contrary to the speculation based on earlier experimental data. The ratio of entry length in an elliptical duct to that in a circular duct with radius equal to the semi-major axis of the elliptical duct is nearly equal to the aspect ratio of the duct. In conformity with the previous work, the present results find the total pressure defect to be independent of the aspect ratio, with a value of 1·234.

KEY WORDS Entrance flow Elliptical duct

1. INTRODUCTION

It is well known that an external flow over a cylinder of elliptical cross-section experiences less pressure drop than that over a cylinder of circular cross-section. This has led to the manufacture of heat exchangers with elliptical tubes. For the optimization of these heat exchangers, accurate information regarding flow and temperature development in the entrance region of elliptical ducts is essential, specially when the tubes are of short length.

Toa[1] presented closed-form solution for the laminar fully developed velocity profile in elliptical ducts using complex variable approach. Lundgren *et al.*[2] devised an approximate method to determine the pressure defect in the entrance region due to increased friction and momentum of the fluid. Later McComas[3] extended the analysis of Lundgren *et al.*[2] to predict the hydrodynamic entrance length. Chiranjivi and Prasad[4] measured friction factors in three elliptical ducts with aspect ratio 0·25, 0·5 and 0·75. Shah and London[5] pointed out that the straight duct upstream of the test section of Reference 4 was of insufficient length for the flow to be fully developed. Consequently, the results of Reference 4 are valid neither for the developing region nor for the fully developed region. Later Rao *et al.*[6] compared their experimental data for fully developed

0271–2091/93/241079–18$14.00

Received November 1992
Revised August 1993

friction factor for aspect ratio 0·25 with the analytical results, and found the difference to be ±10 per cent.

Bhatti[7] was perhaps the first to predict the developing axial velocity and pressure distribution in the entrance region of elliptical ducts. He presented closed-form solutions using the Karman–Pohlhausen integral method. This method requires the velocity profile within the boundary layer as well as axial growth of the boundary layer thickness to be assumed for a three-dimensional flow. Bhatti[7] assumed the ratio of boundary layer thickness along the minor and major axes to be equal to the aspect ratio of the duct throughout the entrance length. This assumption is correct for a circular duct (where the aspect ratio is unity and the flow is symmetric) and becomes increasingly poor as the aspect ratio deviates from unity, specially near the duct entrance. Bhatti also assumed that at the duct inlet the streamwise growth of boundary layer is identical to that on a flat plate at zero incidence. However, while the former is influenced by the favourable pressure gradient, the latter has no pressure gradient.

Later Garg and Velusamy[8] developed an approximate numerical model to eliminate the assumption made by Bhatti[7] regarding the streamwise growth of the boundary layer. Their model is approximate in the sense that they did not solve all the three momentum equations. They found that the entrance lengths predicted by Bhatti[7] are larger for aspect ratios close to unity and shorter for aspect ratios away from unity. They also found the total pressure defect to be a weak monotonic function of the aspect ratio. However, Bhatti's analysis predicts it to be 7/6 for any aspect ratio. Garg and Velusamy[8] also compared their numerical results with the experimental data of Abdel-Wahed *et al.*[9] for aspect ratio of 0·5 at some axial locations. They found a good comparison for the velocity profiles but not so good for the pressure distribution. It was felt that the discrepancy could be due to the approximate nature of the analysis,[8] and a more rigorous numerical model ought to be adopted. Herein, we present a numerical solution for this complex three-dimensional flow by solving all the three momentum equations along with the continuity equation for various aspect ratios of the duct.

2. ANALYSIS

Consider an incompressible, Newtonian fluid entering a straight duct of elliptical cross-section. We assume negligible body forces and laminar flow with constant properties. In conformity with existing developing flow solutions in straight ducts, momentum diffusion in the axial direction is neglected in comparison with that in the cross-stream direction. This assumption renders the governing equations parabolic in the axial direction. We use elliptic cylinder co-ordinates (ξ, η, z) as shown in Figure 1. This co-ordinate system consists of an orthogonal family of confocal ellipses and hyperbolas in a plane, translated in the third (axial here) direction normal to the plane. The surfaces $\eta = \text{constant}$ are the confocal elliptic cylinders

$$\frac{x^2}{(c\cosh\eta)^2}+\frac{y^2}{(c\sinh\eta)^2}=1,$$

while the surfaces $\xi = \text{constant}$ are the hyperbolic cylinders

$$\frac{x^2}{(c\cos\xi)^2}-\frac{y^2}{(c\sin\xi)^2}=1.$$

The normalized equations for conservation of mass and momentum are[10]

$$\frac{1}{H^2}\frac{\partial}{\partial\xi}(HU)+\frac{1}{H^2}\frac{\partial}{\partial\eta}(HV)+\frac{\partial W}{\partial Z}=0, \tag{1}$$

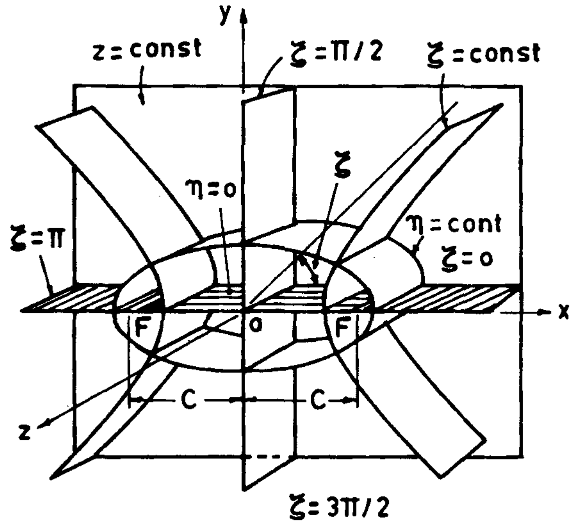

Figure 1. Elliptic-cylinder co-ordinate system

$$\frac{1}{H^2}\frac{\partial}{\partial\xi}(HU^2)+\frac{1}{H^2}\frac{\partial}{\partial\eta}(HUV)+\frac{\partial}{\partial Z}(UW)=\frac{1}{H^2}\left[\frac{\partial^2U}{\partial\xi^2}+\frac{\partial^2U}{\partial\eta^2}\right]-\frac{1}{H}\frac{\partial P'}{\partial\xi}$$

$$+\frac{1}{H^2}\left[\frac{2}{H}\frac{\partial V}{\partial\xi}\frac{\partial H}{\partial\eta}-\frac{2}{H}\frac{\partial V}{\partial\eta}\frac{\partial H}{\partial\xi}-\frac{U}{H}\left(\frac{\partial^2H}{\partial\xi^2}+\frac{\partial^2H}{\partial\eta^2}\right)\right]+\frac{V}{H^2}\left(V\frac{\partial H}{\partial\xi}-U\frac{\partial H}{\partial\eta}\right), \tag{2a}$$

$$\frac{1}{H^2}\frac{\partial}{\partial\xi}(HUV)+\frac{1}{H^2}\frac{\partial}{\partial\eta}(HV^2)+\frac{\partial}{\partial Z}(VW)=\frac{1}{H^2}\left[\frac{\partial^2V}{\partial\xi^2}+\frac{\partial^2V}{\partial\eta^2}\right]-\frac{1}{H}\frac{\partial P'}{\partial\eta}$$

$$+\frac{1}{H^2}\left[\frac{2}{H}\frac{\partial U}{\partial\eta}\frac{\partial H}{\partial\xi}-\frac{2}{H}\frac{\partial U}{\partial\xi}\frac{\partial H}{\partial\eta}-\frac{V}{H}\left(\frac{\partial^2H}{\partial\xi^2}+\frac{\partial^2H}{\partial\eta^2}\right)\right]+\frac{U}{H^2}\left(U\frac{\partial H}{\partial\eta}-V\frac{\partial H}{\partial\xi}\right), \tag{2b}$$

$$\frac{1}{H^2}\frac{\partial}{\partial\xi}(HUW)+\frac{1}{H^2}\frac{\partial}{\partial\eta}(HVW)+\frac{\partial}{\partial Z}(W^2)=\frac{1}{H^2}\left[\frac{\partial^2W}{\partial\xi^2}+\frac{\partial^2W}{\partial\eta^2}\right]-\frac{\partial\bar{P}}{\partial Z}. \tag{2c}$$

The integral form of the continuity equation at any duct cross-section is

$$\int_{\xi=0}^{\pi/2}\int_{\eta=0}^{\eta_w} WH^2\,\mathrm{d}\xi\,\partial\eta=\frac{[E(m)]^2}{4\pi\lambda}. \tag{3}$$

In equations (2a)–(2c) the pressure field $P(\xi,\eta,Z)$ has been split into two parts such that

$$P(\xi,\eta,Z)=\bar{P}(Z)+P'(\xi,\eta).$$

This approximation has been used extensively for parabolic confined flows.

Due to symmetry only a quarter of the duct needs to be considered for the analysis. Hence, the boundary conditions to be imposed are

$$\begin{aligned}
&U=\frac{\partial V}{\partial \xi}=\frac{\partial W}{\partial \xi}=0 \quad \text{along } \xi=0, \pi/2 && \text{for all } \eta \text{ and } Z,\\
&\frac{\partial U}{\partial \eta}=V=\frac{\partial W}{\partial \eta}=0 \quad \text{along } \eta=0 && \text{for all } \xi \text{ and } Z,\\
&U=V=W=0 \quad \text{along } \eta=\eta_W && \text{for all } \xi \text{ and } Z,\\
&U=V=\bar{P}=0 \quad \text{and } W=1 \text{ at } Z=0 && \text{for all } \xi \text{ and } \eta.
\end{aligned} \tag{4}$$

Equations (1)–(4) form a complete set of equations for the three components of velocity and two parts of pressure. The pressure defect, K, at any axial location is given by

$$K(Z)=2\left[\left(\frac{\mathrm{d}P}{\mathrm{d}Z}\right)_{\mathrm{f}} Z-\bar{P}(Z)\right],$$

where $(\mathrm{d}P/\mathrm{d}Z)_{\mathrm{f}}$ is the fully developed pressure gradient in the duct.

3. SOLUTION

Since no analytical solution is known to this set of non-linear, interlinked partial differential equations, numerical solution is resorted to. The control volume-based discretization method[11] has been used. The discretization equations are given in the Appendix II. The solution at any marching axial location is obtained in two stages. The first stage contains the solution for axial velocity component and duct average pressure from equations (2c) and (3). The second stage contains the solution for cross-stream velocity components and deviational pressure from equations (1), (2a) and (2b). At any axial marching location these two stages are repeated sufficiently to account for non-linearity and interlinkage of the equations. The procedure adopted for the solution is a modified form of Patankar and Spalding's method[12] for parabolic flows. The major modifications include (i) use of SIMPLER algorithm[11] for resolving the cross-stream pressure–velocity coupling and (ii) use of Raithby and Schneider's method[13] for evaluating the axial pressure gradient. During discretization of the governing equations, the convection and diffusion fluxes are combined using upwind scheme.[11] Power-law scheme[11] was also used initially in some cases to check if any undue numerical diffusion is present in the use of upwind scheme. A maximum difference of ~3 per cent was found in pressure and pressure defect very close to the entrance, with much less difference away from the entrance. The maximum difference in the centreline velocity was only 0·3 per cent. The difference in the flow development length between the two schemes is 0·9 per cent. Hence, only upwind scheme was used for all subsequent calculations and for the results given here.

The discretization procedure yields a set of algebraic equations for each variable. The pentadiagonal system of algebraic equations for each variable is solved by a plane-by-plane method.[14,15] This method is an extension of the Thomas algorithm for the tridiagonal system of equations. Convergence at any marching step is assumed once the absolute sum of the residue R_ϕ corresponding the variable ϕ in the discretization equation is less than ε, where

$$R_\phi=\sum_{i=1}^{n_\phi}|r_{i\phi}|.$$

The value of ε is taken to be 5×10^{-5} for cross-stream equations and 10^{-5} for axial momentum and integral continuity equations. No significant change in the results was observed when the value of ε for cross-stream equations was reduced to 10^{-5}.

In the cross-stream (ξ–η) plane, a 22×25 non-uniform grid pattern was used for $\lambda \leq 0{\cdot}5$. For $\lambda = 0{\cdot}7$ and 0·9, grid patterns of 19×25 and 22×28, respectively, were used. Grids were packed near the duct wall where large velocity gradients persist. A grid independency test was also conducted. A grid pattern of 13×16 (with grid sizes nearly double that of the 22×28 grid) was also used for $\lambda = 0{\cdot}9$. The maximum differences in the centreline axial velocity, average pressure in the duct, pressure defect and flow development length computed using the two grid patterns are 0·4, 1·4, 1·9 and 1·2 per cent, respectively. Hence, the grid size selected is satisfactory.

In the axial direction very fine grids of size 10^{-6} were used near the duct entrance for all aspect ratios except for $\lambda = 0{\cdot}1$ where it was 10^{-7}. As the flow developed, the step size was gradually increased to 10^{-4}, 10^{-4}, 5×10^{-5}, 2×10^{-5} and 5×10^{-6}, respectively, for $\lambda = 0{\cdot}9$, 0·7, 0·5, 0·3 and 0·1. The total number of axial steps used were 1396, 1590, 2736, 4824 and 25108, respectively, for $\lambda = 0{\cdot}9$, 0·7, 0·5, 0·3 and 0·1. Relaxation factors of 0·8 for the momentum equations and 0·6 for pressure equations were used. The flow was assumed to be fully developed once the centreline axial velocity reached 99 per cent of the fully developed value.

4. ACCURACY

In order to validate the computer program, the well-studied problem of flow development in a circular pipe was computed first. The aspect ratio for this study was taken to be 0·999 since the co-ordinate transformation does not hold for $\lambda = 1$. The computed results of axial velocity at various radial positions, duct average pressure and pressure defect as a function of axial location were compared with the numerical results of Hornbeck[16] for a circular pipe. The present axial velocity was found to match very well with Hornbeck's values[16] in the entire duct. For the average pressure, a maximum difference of 2·7 per cent was observed close to the entrance, and it was much less away from the entrance. The pressure defect predicted by Hornbeck[16] was found to be higher than the present value by 2·5 per cent.

As another validation, fully developed flow velocity and pressure gradient in elliptical ducts were obtained for various values of the aspect ratio. These values were compared against the analytical result.[5,7] The fully developed velocity profile is given by[7]

$$W = 2(1 - X^2 - Y^2). \tag{5}$$

The present results for both velocity and axial pressure gradient match very well with the analytical results.

5. RESULTS AND DISCUSSION

Results were obtained for five values of the aspect ratio, $\lambda = 0{\cdot}9$, 0·7, 0·5, 0·3 and 0·1. However, for brevity, results for $\lambda = 0{\cdot}7$ and 0·3 are not presented here. Results for the rest three aspect ratios are presented in the following form:

(i) development of axial velocity component along the minor axis with y/b as a parameter,
(ii) development of axial velocity component along the major axis with x/a as a parameter,
(iii) isoaxial-velocity-component contours at various axial locations and
(iv) development of duct average pressure, pressure defect and the duct pressure if the flow were fully developed at the entrance itself.

Figures 2(a)–2(c) depict the development of axial velocity along the minor axis for various values of the aspect ratio. It is clear that once the uniform flow enters the duct, fluid adjacent to the duct wall decelerates and that near the centerline accelerates continuously. The fluid at some intermediate location accelerates initially up to a certain axial length while it is in the core region but finally starts to decelerate once it is engulfed in the viscous region. Also shown in Figure 2 are the analytical results of Bhatti.[7] Bhatti's results differ from the present ones in the near-entrance region. In locations close to the duct wall, Bhatti's velocities are overpredicted and, consequently, in locations close to the duct axis they are underpredicted. The degree of this overprediction and underprediction increases as λ decreases. This indicates that the actual boundary layer along the minor axis grows at a faster rate than that assumed by Bhatti. Similar observations on Bhatti's results were made by Garg and Velusamy.[8]

The development of axial velocity along the minor axis of large aspect ratio ducts differs from that of small aspect ratio ducts. For example, let us compare Figures 2(a) and 2(c) corresponding to $\lambda = 0{\cdot}9$ and $0{\cdot}1$, respectively. In Figure 2(a) at locations $y/b = 0{\cdot}6$ and $0{\cdot}7$, the velocity increases initially for low Z-values when the fluid is in the core region and reaches a maximum. Then it starts to reduce as Z increases further. However, this is not completely true for $\lambda = 0{\cdot}1$. Here also the velocity increases initially, reaches a maximum and then drops. But it increases again after a certain Z-value. This secondary increase is due to the efflux of fluid from the boundary layer developing along the major axis, with the relative growth rate of the boundary layer along the major axis, δ/a, being slower than that along the minor axis, δ/b. Such a secondary increase in velocity is not observed for aspect ratios close to unity where the boundary layer growth rates along the major and minor axes are nearly equal.

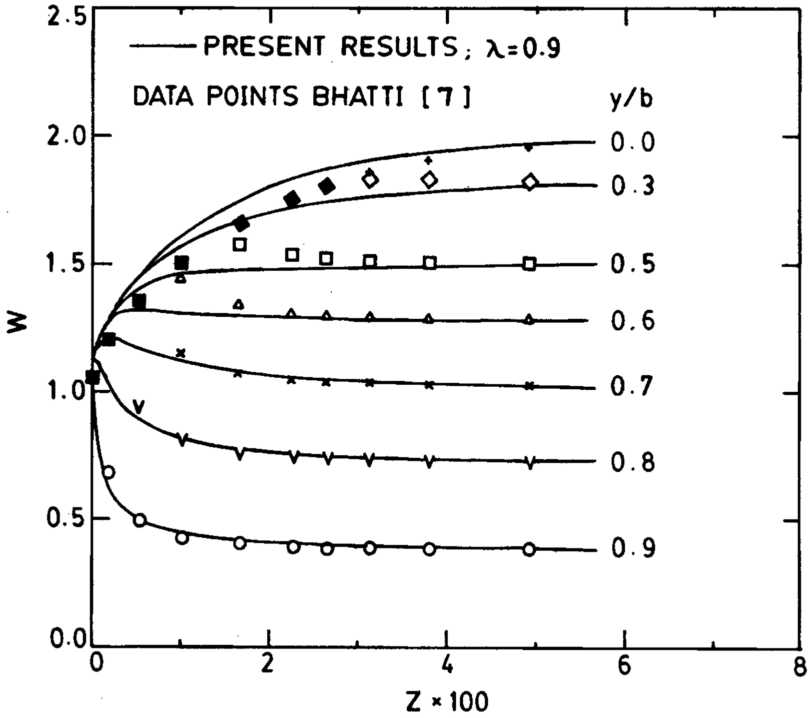

Figure 2(a). Development of axial velocity along the minor axis for $\lambda = 0{\cdot}9$

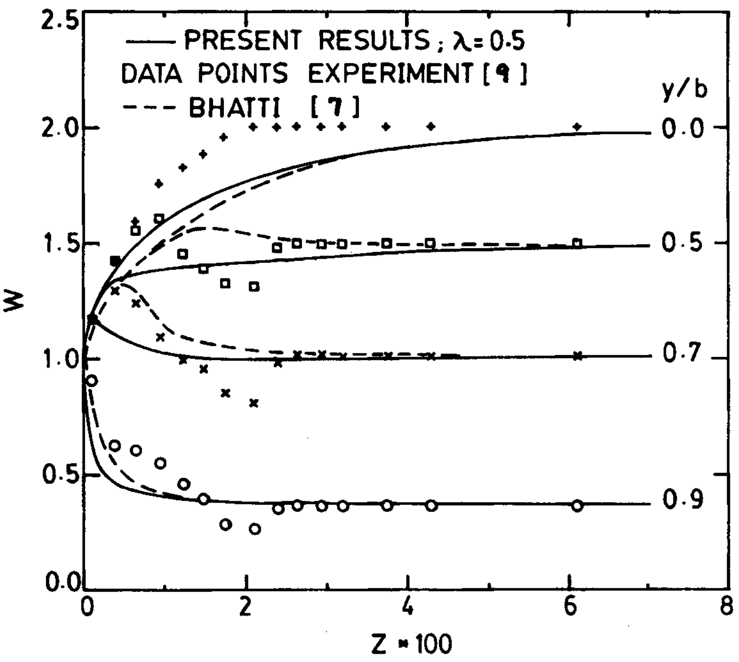

Figure 2(b). Development of axial velocity along the minor axis for $\lambda = 0{\cdot}5$

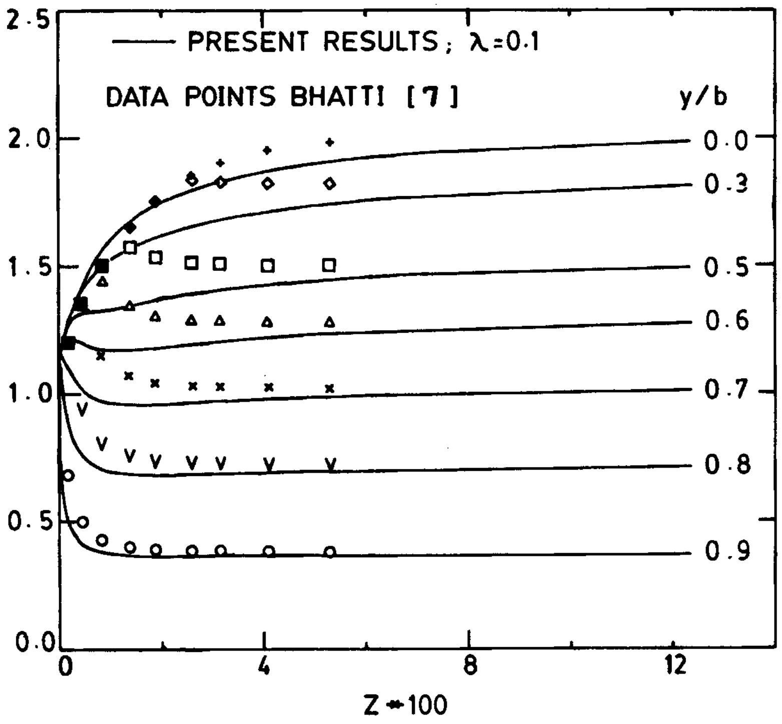

Figure 2(c). Development of axial velocity along the minor axis for $\lambda = 0{\cdot}1$

Experimental data of Abdel-Wahed *et al.*[9] are also included in Figure 2(b) for $\lambda=0{\cdot}5$. Experimental results do not show a smooth variation of velocity at any y/b location. Abdel-Wahed *et al.*[9] attributed this to the existence of transverse recirculation in the developing region. However, they did not confirm this recirculation by measuring cross-stream velocity components. In the present results we did not find any such recirculation at any point in the duct. We may point out that the present model is capable of predicting any transverse recirculation. The parabolic assumption in the axial momentum equation breaks down only if the axial velocity component is negative, implying separated flow. Such a situation is not physical. Near the duct entrance ($Z<0{\cdot}02$) the present results differ from the experimental data considerably but beyond $Z=0{\cdot}02$ the comparison is satisfactory.

Development of axial velocity along the major axis for various values of the aspect ratio is shown in Figures 3(a)–3(c). Comparison of Figure 3 with the corresponding Figure 2 reveals that the flow along the major axis develops at a slower rate than that along the minor axis. Also, this difference in the development rate increases as λ decreases. This result is contrary to the assumption made by Bhatti[7] and Garg and Velusamy.[8] Bhatti's results are also presented in Figure 3. Clearly, Bhatti's results for axial velocity along the major axis are generally underpredicted, specially for $\lambda<0{\cdot}7$. Also the degree of underprediction increases as λ decreases. This indicates that the actual boundary layer growth along the major axis is slower than that assumed by Bhatti.[7]

Experimental data of Abdel-Wahed *et al.*[9] are also presented in Figure 3(b) for $\lambda=0{\cdot}5$. The non-smooth variation of experimental data was again attributed to transverse recirculation. As

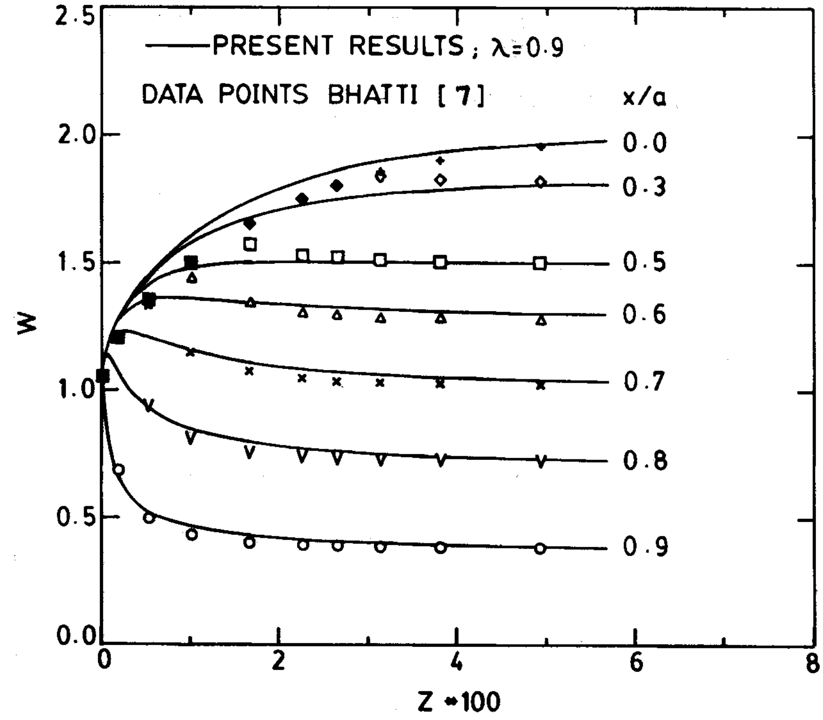

Figure 3(a). Development of axial velocity along the major axis for $\lambda = 0{\cdot}9$

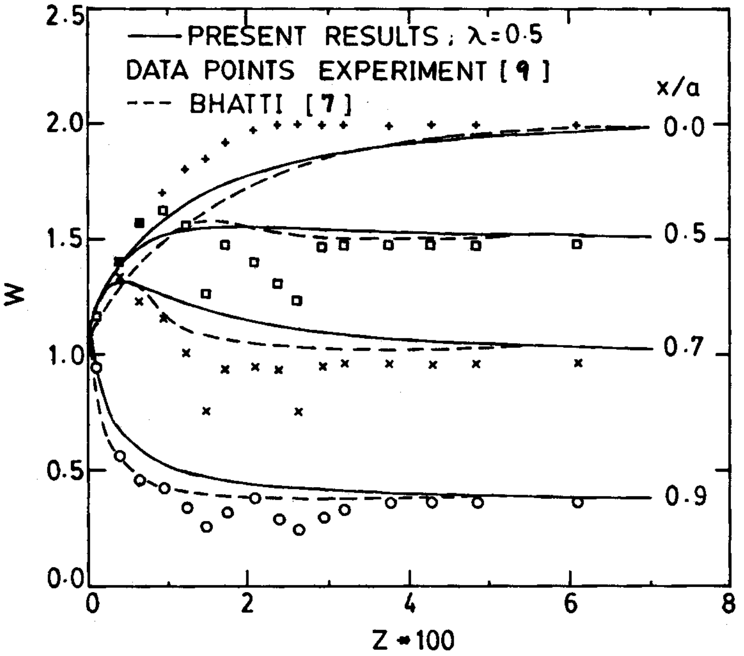

Figure 3(b). Development of axial velocity along the major axis for $\lambda = 0{\cdot}5$

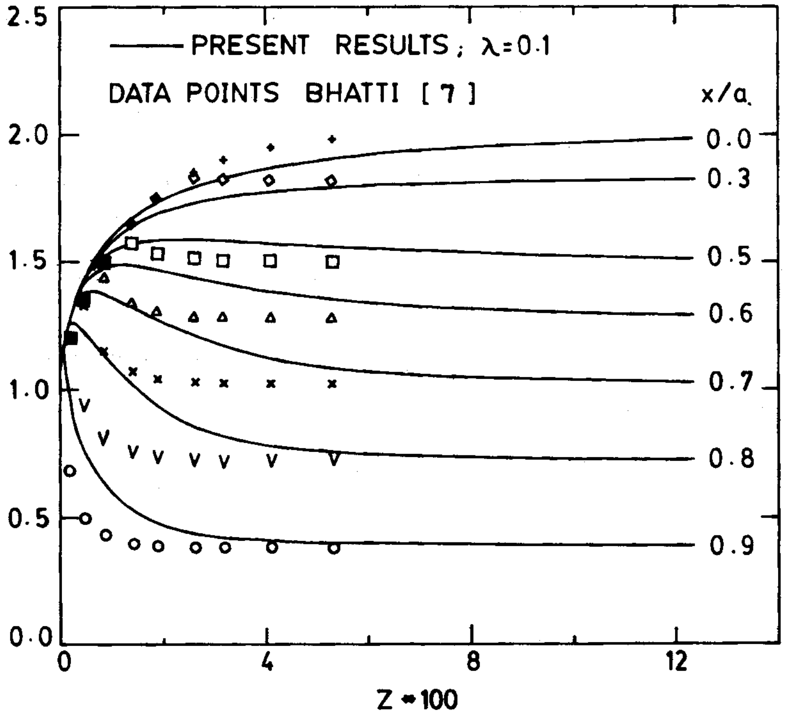

Figure 3(c). Development of axial velocity along the major axis for $\lambda = 0{\cdot}1$

already pointed out no such recirculation is observed in the present results. The present results differ considerably from the experimental data in the region $Z<0{\cdot}03$ but beyond this region the comparison is somewhat satisfactory. Table I compares the fully developed velocity values from the present computations and the experimental data[9] with the analytical values from equation (5) for $\lambda=0{\cdot}5$. The experimental values are less than the analytical values with a maximum difference of 12·1 per cent for $x/a=0{\cdot}8$. A deviation of about 1 per cent is expected in the present results since the flow is assumed to be fully developed once the centreline velocity reaches 99 per cent of the fully developed value.

Figures 4(a) and 4(b) show contours of axial velocity component at six different axial locations in the duct for $\lambda=0{\cdot}9$ and 0·5, respectively. From Figure 4(a), it is clear that the maximum axial velocity increases from 1·1 at $Z=0{\cdot}0003$ to 1·9 at $Z=0{\cdot}032$. Also the contours are tightly packed near the duct wall at $Z=0{\cdot}0003$, indicating sharp velocity and pressure gradients. Moreover, they become increasingly sparse and approach fully developed contours as Z increases. These observations are true for Figure 4(b) as well. We may mention that similar contours were found for other aspect ratios. However, while the axial velocity contours in Figure 4(a) are nearly concentric ellipses, those in Figure 4(b) are not. Thus, the assumption of Bhatti[7] and Garg and Velusamy[8] regarding the velocity profiles in the developing region is not correct for values of λ away from unity.

The duct average pressure, the pressure defect and the duct pressure if the flow were fully developed from $Z=0$ onwards are shown in Figures 5(a)–5(c) for various λ-values. The pressure gradient is the maximum at the entrance due to steep velocity gradient near the wall in this region, and it slowly approaches the fully developed value as Z increases. The pressure defect also increases sharply near the entrance and attains a constant value once the flow is fully developed. Figure 5 also contain Bhatti's results[7] for all aspect ratios and experimental data[9] for $\lambda=0{\cdot}5$. It is clear that the pressure gradient and consequently the pressure defect estimated by Bhatti's model are slightly higher than the present values near the entrance. This is true for all aspect ratios. Also, the measured pressure gradient and the pressure defect are much less than the theoretical values very close to the entrance. However, at full development of the flow, the measured pressure defect is higher than the theoretical value.

The pressure defect at $Z=Z_\infty$ was found to be almost independent of λ, having a value of 1·234. The same estimated by Bhatti[7] and Lundgren *et al.*[2] is 7/6 and 4/3, respectively. The present value lies between the two. It is known[8] that the value of Lundgren *et al.*[2] is overpredicted. In their approximate numerical analysis, Garg and Velusamy[8] found the total pressure defect to be

Table I. Analytical, numerical and experimental values of fully developed axial velocity for $\lambda = 0{\cdot}5$

x/a	Analytical W_f	Present results		Experimental[9]	
		W_∞	% Differ. from W_f	W_∞	% Differ. from W_f
0·9	0·38	0·383	0·8	0·362	4·7
0·8	0·72	0·728	1·1	0·633	12·1
0·7	1·02	1·025	0·5	0·957	6·2
0·6	1·28	1·290	0·8	1·223	4·5
0·5	1·50	1·507	0·5	1·468	2·1
0·4	1·68	1·681	0·1	1·660	1·2
0·2	1·92	1·905	0·8	1·894	1·4

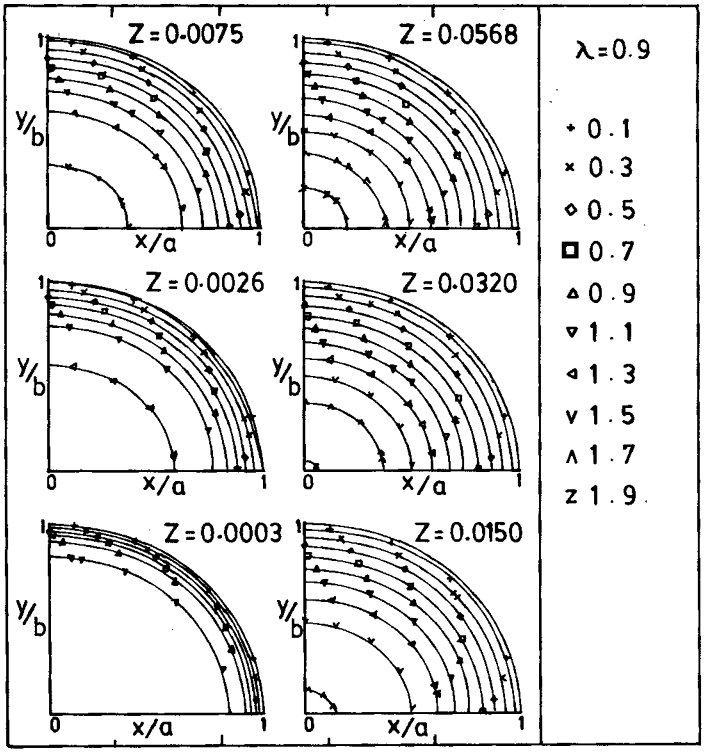

Figure 4(a). Constant axial velocity contours for $\lambda = 0{\cdot}9$

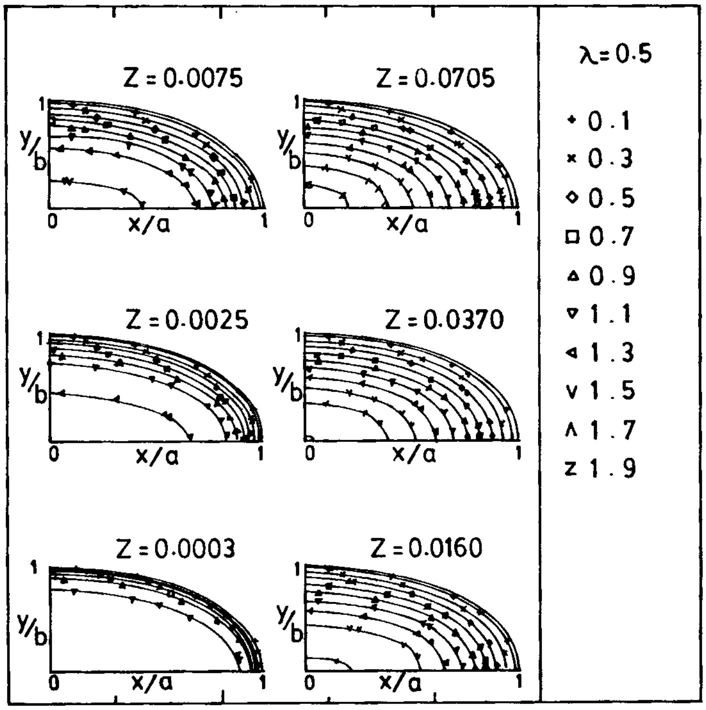

Figure 4(b). Constant axial velocity contours for $\lambda = 0{\cdot}5$

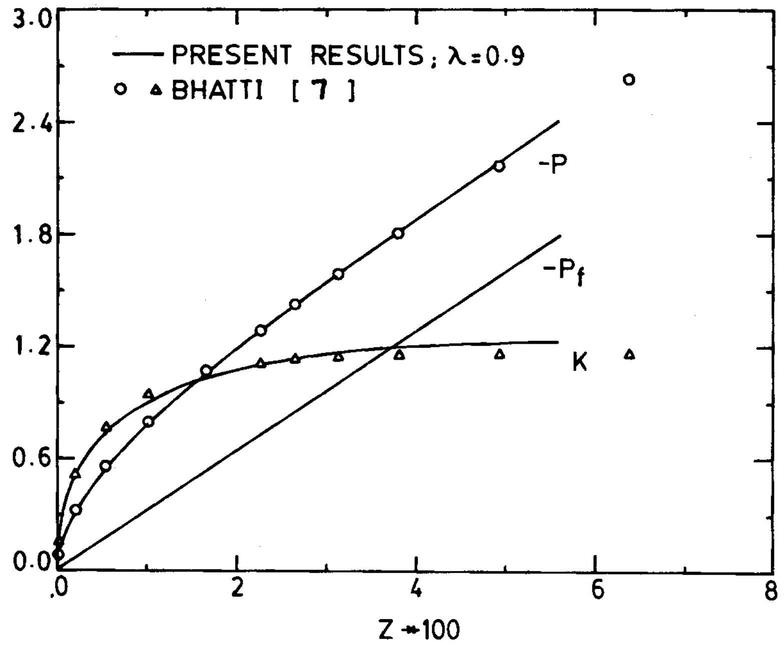

Figure 5(a). Development of axial pressure and pressure defect for $\lambda = 0{\cdot}9$

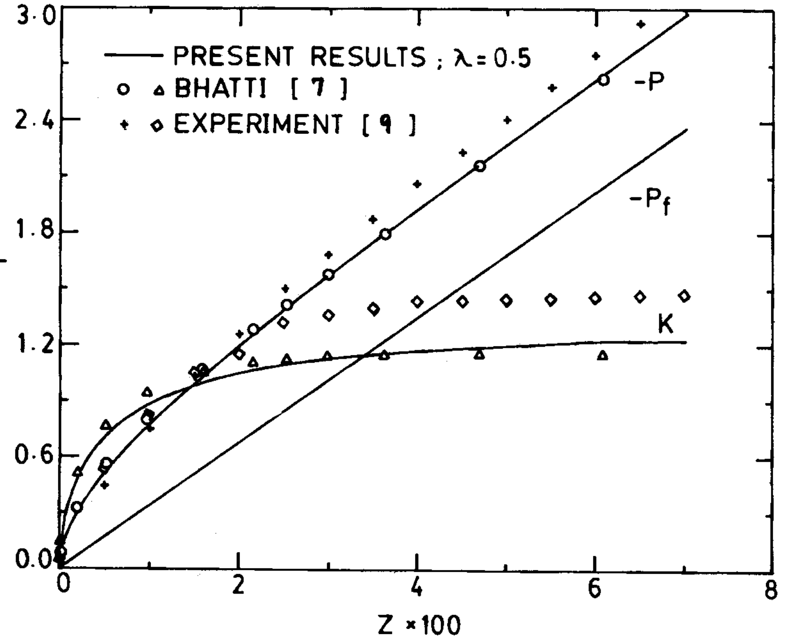

Figure 5(b). Development of axial pressure and pressure defect for $\lambda = 0{\cdot}5$

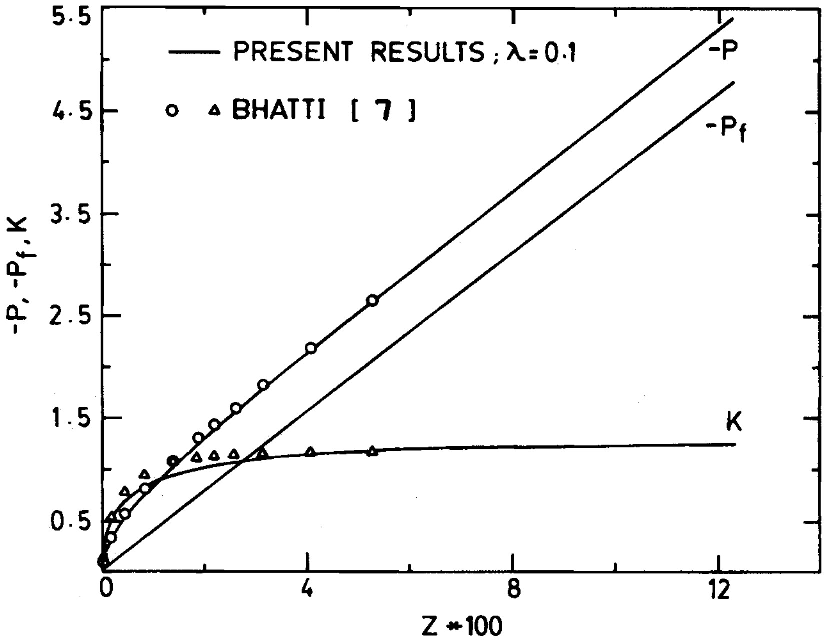

Figure 5(c). Development of axial pressure and pressure defect for $\lambda = 0{\cdot}1$

Table II. Development length (Z_∞)

λ	Present values		Z_∞ from Bhatti[7]
	Z_∞	$z_\infty/z_{\infty c}$	
0·1	0·1234	0·053	0·0531
0·3	0·0925	0·307	0·0574
0·5	0·0703	0·531	0·0610
0·7	0·0605	0·725	0·0632
0·9	0·0568	0·914	0·0641
0·999	0·0557	1·0	0·0642

a weak function of λ, varying from 1·16 to 1·06 for $\lambda = 0{\cdot}91$ to 0·5. The experimental value[9] is 1·395 which is even higher than that of Reference 2.

Table II contains the dimensionless development length Z_∞ and the ratio of development length in an elliptic duct, z_∞, to that in a circular duct, $z_{\infty c}$, with radius equal to the semi-major axis of the elliptical duct for various values of λ. As the duct cross-section becomes more and more elliptic, i.e. as λ decreases, the development length decreases as can be seen from the ratio $z_\infty/z_{\infty c}$. This is due to the fact that as λ decreases, the hydraulic diameter decreases, and thus the flow becomes developed over shorter lengths. It is interesting to note that the ratio $z_\infty/z_{\infty c}$ is nearly equal to λ, except for $\lambda = 0{\cdot}1$. The values of development length due to Bhatti[7] are also given in Table II. Bhatti's values are lower for $\lambda < 0{\cdot}7$ and the difference is as much as 57 per cent for $\lambda = 0{\cdot}1$. However, for $\lambda \geq 0{\cdot}7$, Bhatti's results overpredicted the development length by as much 15 per cent. A similar observation regarding Bhatti's values was made by Garg and Velusamy.[8]

6. CONCLUSIONS

The problem of laminar, three-dimensional flow development in the entrance region of ducts having elliptical cross-section has been solved using the complete Navier–Stokes equations. Numerical results are compared with earlier numerical and experimental data. The following conclusions are drawn:

- (i) The relative growth rate of boundary layer thickness along the major axis of the duct is slower than that along the minor axis.
- (ii) In the developing region, the isoaxial-velocity contours are not concentric ellipses contrary to such an assumption in the earlier analyses.
- (iii) The fully developed value of the pressure defect is almost independent of the duct aspect ratio and equal to 1·234.
- (iv) The smaller the aspect ratio, the shorter is the development length. Also, the ratio of development length in an elliptical duct to that in a circular duct with radius equal to the semi-major axis of the elliptical duct is nearly equal to the aspect ratio for all $\lambda \geq 0{\cdot}3$.
- (v) Although the local velocity values predicted by the momentum integral method[7] are in substantial error, the duct average pressure and pressure defect are quite reasonable.

APPENDIX I: NOMENCLATURE

a	semi-major axis of the elliptical section
b	semi-minor axis of the elliptical section
c	focal distance of the elliptical section
D_h	hydraulic diameter of the elliptical section
$E(m)$	complete elliptic integral of second kind
H	$(c/D_h)(\sinh^2\eta+\sin^2\xi)^{1/2}$
K	pressure defect
m	$(1-\lambda^2)^{1/2}$
n_ϕ	number of control volumes in the cross-section for the variable ϕ
p	total dimensional pressure (function of ξ, η, z)
P	total dimensionless pressure $[=p/(\rho w_e^2)]$
$\bar{p}$	dimensional duct pressure averaged over the cross-section
$\bar{P}$	dimensionless duct pressure $[=\bar{p}/(\rho w_e^2)]$ averaged over the cross-section
p'	dimensional deviational pressure (function of ξ, η)
P'	dimensionless deviational pressure $[=p'D_h^2/(\rho\nu^2)]$
$r_{i\phi}$	residue of the discretized equation for ith control volume for the variable ϕ
Re	Reynolds number $(=w_e D_h/\nu)$
R_ϕ	absolute sum of $r_{i\phi}$ taken over n_ϕ
u	velocity component in the ξ-direction
U	dimensionless counterpart of u $(=uD_h/\nu)$
v	velocity component in the η-direction
V	dimensionless counterpart of v $(=vD_h/\nu)$
w	velocity component in the z-direction
w_e	uniform axial velocity at the entrance
W	dimensionless counterpart of w $(=w/w_e)$
x	cross-stream Cartesian co-ordinate (Figure 1)
X	dimensionless co-ordinate $(=x/a)$
y	cross-stream Cartesian co-ordinate (Figure 1)

Y	dimensionless co-ordinate ($=y/b$)
z	axial co-ordinate (Figure 1)
Z	dimensionless axial co-ordinate [$=z/(D_h Re)$]

Greek letters

δ	boundary layer thickness
ε	a small number for checking convergence
η	elliptic cylinder co-ordinate (Figure 1)
λ	aspect ratio of the duct ($=b/a$)
ν	kinematic viscosity of the fluid
ρ	density of the fluid
ξ	elliptic cylinder co-ordinate (Figure 1)

Subscripts

c	value corresponding to a circular duct
f	value corresponding to 100 per cent fully developed flow
w	value at the duct wall
∞	value at an axial location where the centreline axial velocity is 99 per cent of the fully developed value
ϕ	value pertaining to the variable ϕ

APPENDIX II

The discretization equations are derived by integrating the governing partial differential equations over their respective control volumes. The control volumes corresponding to the cross-stream velocity components, U and V, are staggered in their respective directions, ξ and η, as shown in Figure 6.

Integration of ξ-momentum equation (2a) over the control volume surrounding point e in Figure 6, i.e. over the control volume extending from ξ_{P} to ξ_{E}, η_{se} to η_{ne}, and Z_{u} to Z_{d} (where subscripts u and d denote upstream and downstream locations, respectively) yields

$$(J_{\mathrm{E}}-J_{\mathrm{P}})+(J_{\mathrm{ne}}-J_{\mathrm{se}})+(J_{\mathrm{de}}-J_{\mathrm{ue}})=(P'_{\mathrm{P}}-P'_{\mathrm{E}})\bar{H}\,\Delta\eta\,\Delta Z+\bar{S}_{\xi}, \tag{6}$$

where the fluxes J are given by

$$J_{\mathrm{E}}=\left[HU^2-\frac{\partial U}{\partial \xi}\right]_{\mathrm{E}}\Delta\eta\,\Delta Z, \qquad J_{\mathrm{P}}=\left[HU^2-\frac{\partial U}{\partial \xi}\right]_{\mathrm{P}}\Delta\eta\,\Delta Z,$$

$$J_{\mathrm{ne}}=\left[HVU-\frac{\partial U}{\partial \eta}\right]_{\mathrm{ne}}\Delta\xi\,\Delta Z, \qquad J_{\mathrm{se}}=\left[HVU-\frac{\partial U}{\partial \eta}\right]_{\mathrm{se}}\Delta\xi\,\Delta Z,$$

$$J_{\mathrm{de}}=[WU]_{\mathrm{de}}\bar{H}^2\Delta\xi\,\Delta\eta, \qquad J_{\mathrm{ue}}=[WU]_{\mathrm{ue}}\bar{H}^2\Delta\xi\,\Delta\eta,$$

and the source term $\bar{S}_{\xi}$ is given later. Integration of continuity equation (1) over the same control volume, multiplication by U_{e}, and subtraction from equation (6) yields

$$[J_{\mathrm{E}}-F_{\mathrm{E}}U_{\mathrm{e}}]-[J_{\mathrm{P}}-F_{\mathrm{P}}U_{\mathrm{e}}]+[J_{\mathrm{ne}}-F_{\mathrm{ne}}U_{\mathrm{e}}]-[J_{\mathrm{se}}-F_{\mathrm{se}}U_{\mathrm{e}}]+[J_{\mathrm{de}}-F_{\mathrm{de}}U_{\mathrm{e}}]-[J_{\mathrm{ue}}-F_{\mathrm{ue}}U_{\mathrm{e}}]$$
$$=(P'_{\mathrm{P}}-P'_{\mathrm{E}})\bar{H}\Delta\eta\,\Delta Z+\bar{S}_{\xi}. \tag{7}$$

where the F's are defined later. From the generalized formulation for combining the convective

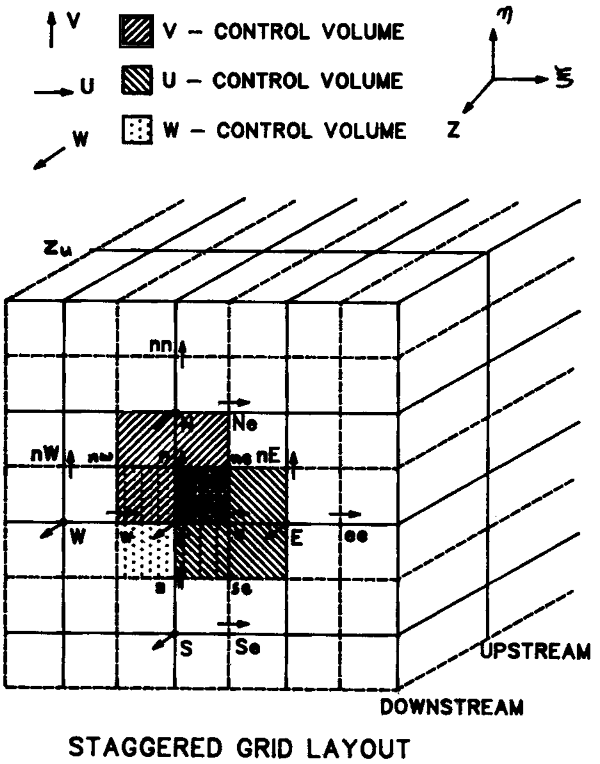

Figure (6). Staggered grid layout.

and diffusive fluxes (Reference 11, p. 99), equation (7) reduces to

$$a_e U_e = a_{ee} U_{ee} + a_w U_w + a_{Ne} U_{Ne} + a_{Se} U_{Se} + a_{ue} U_{ue} + (P'_P - P'_E)\bar{H}\,\Delta\eta\,\Delta Z + \bar{S}_\xi, \tag{8}$$

where

$$a_{ee} = D_E A(|P_E|) + [\![-F_E, 0]\!], \quad F_E = (HU)_E\,\Delta\eta\,\Delta Z, \quad D_E = \frac{\Delta\eta\,\Delta Z}{\Delta\xi}, \quad P_E = \frac{F_E}{D_E},$$

$$a_w = D_P A(|P_P|) + [\![F_P, 0]\!], \quad F_P = (HU)_P\,\Delta\eta\,\Delta Z, \quad D_P = \frac{\Delta\eta\,\Delta Z}{\Delta\xi}, \quad P_P = \frac{F_P}{D_P},$$

$$a_{Ne} = D_{ne} A(|P_{ne}|) + [\![-F_{ne}, 0]\!], \quad F_{ne} = (HV)_{ne}\,\Delta\xi\,\Delta Z, \quad D_{ne} = \frac{\Delta\xi\,\Delta Z}{\Delta\eta}, \quad P_{ne} = \frac{F_{ne}}{D_{ne}},$$

$$a_{Se} = D_{se} A(|P_{se}|) + [\![F_{se}, 0]\!], \quad F_{se} = (HV)_{se}\,\Delta\xi\,\Delta Z, \quad D_{se} = \frac{\Delta\xi\,\Delta Z}{\Delta\eta}, \quad P_{se} = \frac{F_{se}}{D_{se}},$$

$$a_{ue} = W_{ue}\bar{H}^2\,\Delta\xi\,\Delta\eta, \qquad a_e = a_{ee} + a_w + a_{Ne} + a_{Se} + a_{ue},$$

$$\bar{S}_\xi = \left(\overline{\frac{2}{H}\frac{\partial H}{\partial\eta}}\right)(V_E - V_P)\,\Delta\eta\,\Delta Z - \left(\overline{\frac{2}{H}\frac{\partial H}{\partial\xi}}\right)(V_{ne} - V_{se})\,\Delta\xi\,\Delta Z + \Delta\xi\,\Delta\eta\,\Delta Z$$

$$\left[\left(\overline{\frac{\partial H}{\partial\xi}}\right)\overline{V_e^2} - \left(\overline{\frac{\partial H}{\partial\eta}}\right)(\overline{UV})_e - U_e\left\{\overline{\frac{1}{H}\left(\frac{\partial^2 H}{\partial\xi^2} + \frac{\partial^2 H}{\partial\eta^2}\right)}\right\}\right],$$

and the symbol $[\![\ ]\!]$ indicates the maximum of the values contained. The definition of function A depends upon the scheme used in Reference 11. For example, for the upwind scheme $A=1$, while for the power-law scheme $A=[\![0,(1-0{\cdot}1|P|)^5]\!]$.

Similarly, the discretization equation for η-momentum can be derived by integrating equation (2b) over the control volume surrounding point n in Figure 6 to yield

$$a_n V_n = a_{nE} V_{nE} + a_{nW} V_{nW} + a_{nn} V_{nn} + a_s V_s + a_{un} V_{un} + (P'_P - P'_N)\bar{H}\,\Delta\xi\,\Delta Z + \bar{S}_\eta, \tag{9}$$

where the coefficients a's are similar to those in equation (8), and

$$\bar{S}_\eta = \left(\overline{\frac{2}{H}\frac{\partial H}{\partial \xi}}\right)(U_N - U_P)\,\Delta\xi\,\Delta Z - \left(\overline{\frac{2}{H}\frac{\partial H}{\partial \eta}}\right)(U_{ne} - U_{nw})\,\Delta\eta\,\Delta Z$$
$$+\Delta\xi\,\Delta\eta\,\Delta Z\left[\left(\overline{\frac{\partial H}{\partial \eta}}\right)\overline{U_n^2} - \left(\overline{\frac{\partial H}{\partial \xi}}\right)(\overline{UV})_n - V_n\left\{\overline{\frac{1}{H}\left(\frac{\partial^2 H}{\partial \xi^2} + \frac{\partial^2 H}{\partial \eta^2}\right)}\right\}\right].$$

A similar integration performed in equation (2c) over the control volume surrounding point P in Figure 6 yields

$$a_P W_P = a_E W_E + a_W W_W + a_N W_N + a_S W_S + a_u W_{uP} + \bar{S}_Z, \tag{10}$$

where coefficients a's are similar to those in equation (8), and

$$\bar{S}_Z = -\frac{\partial \bar{P}}{\partial Z}\overline{H^2}\,\Delta\xi\,\Delta\eta\,\Delta Z.$$

The continuity equation (1), upon integration over the control volume surrounding point P in Figure 6, yields

$$[(HU)_e - (HU)_w]\,\Delta\eta\,\Delta Z + [(HV)_n - (HV)_s]\,\Delta\xi\,\Delta Z = -[W_P - W_{uP}]\,\overline{H^2}\,\Delta\xi\,\Delta\eta. \tag{11}$$

It may be noted that a fully implicit procedure is adopted in the parabolic Z-direction. Hence, in equations (8)–(10), the unknowns without the subscript 'u' correspond to the downstream Z-plane and those with the subscript 'u' correspond to the upstream Z-plane.

REFERENCES

1. L. N. Toa, 'On some laminar forced convection problems', *J. Heat Transfer*, **83,** 466–472 (1961).
2. T. S. Lundgren, E. M. Sparrow and J. B. Starr, 'Pressure drop due to the entrance region in ducts of arbitrary cross-section', *J. Basic Eng.*, **86,** 620–626 (1964).
3. S. T. McComas, 'Hydrodynamic entrance lengths for ducts of arbitrary cross section', *J. Basic Eng.*, **89,** 847–850 (1967).
4. C. Chiranjivi and A. R. Prasad, 'Study of laminar flow friction in elliptical conduits', *Indian J. Technol.*, **12,** 87–90 (1974).
5. R. K. Shah and A. L. London, *Laminar Flow Forced Convection in Ducts*, Academic Press, New York, 1978.
6. S. S. Rao, D. C. Raju and M. V. R. Rao, 'Pressure drop studies in elliptical ducts', *Indian J. Technol.*, **13,** 6–11 (1975).
7. M. S. Bhatti, 'Laminar flow in the entrance region of elliptical ducts', *J. Fluids Eng.*, **105,** 290–296 (1983).
8. V. K. Garg and K. Velusamy, 'Developing flow in an elliptical duct', *Int. J. Eng. Fluid Mech.*, **2**(2), 177–196 (1989).
9. R. M. Abdel-Wahed, A. E. Attia and M. A. Hifni, 'Experiments on laminar flow and heat transfer in an elliptical duct', *Int. J. Heat Mass Transfer*, **27,** 2397–2413 (1984).
10. W. F. Hughes and E. W. Gaylord, *Basic Equations of Engineering Science*, McGraw-Hill, New York, 1964.
11. S. V. Patankar, *Numerical Heat Transfer and Fluid Flow*, McGraw-Hill, New York, 1980.
12. S. V. Patankar and D. B. Spalding, 'A calculation procedure for heat, mass and momentum transfer in three-dimensional parabolic flows', *Int. J. Heat Mass Transfer*, **15,** 1787–1806 (1972).
13. G. D. Raithby and G. E. Schneider, 'Numerical solution of problems in incompressible fluid flow: treatment of the velocity-pressure coupling', *Numer. Heat Transfer*, **2,** 417–440 (1979).

14. K. Velusamy, 'Introduction of whole field solution procedure and porous body formulations in THYC-2D', *Internal Note: PFBR/66040/DN/1041/R-A*, IGCAR, 1989.
15. H. I. Rosten and D. B. Spalding, 'PHOENICS – Beginners guide and user manual', *Rep. No. TR/100*, CHAM Ltd., 1986.
16. R. W. Hornbeck, *Numerical Marching Techniques for Fluid Flows With Heat Transfer, NASA SP-297*, Washington, DC, 1973.